Predictive Torque Control of Induction Machines Based on State-Space Models

Hernán Miranda, *Student Member, IEEE*, Patricio Cortés, *Member, IEEE*, Juan I. Yuz, *Member, IEEE*, and José Rodríguez, *Senior Member, IEEE*

***Abstract*—In this paper, we present a predictive control algorithm that uses a state-space model. Based on classical control theory, an exact discrete-time model of an induction machine with time-varying components is developed improving the accuracy of state prediction. A torque and stator flux magnitude control algorithm evaluates a cost function for each switching state available in a two-level inverter. The voltage vector with the lowest torque and stator flux magnitude errors is selected to be applied in the next sampling interval. A high degree of flexibility is obtained with the proposed control technique due to the online optimization algorithm, where system nonlinearities and restrictions can be included. Experimental results for a 4-kW induction machine are presented to validate the proposed state-space model and control algorithm.**

***Index Terms*—Induction motor drives, predictive control, state-space methods.**

I. Introduction

THE constantly increasing need for better industrial drives (fastest dynamic response, parameter robustness, algorithm simplicity, among others) has encouraged researchers to develop new control strategies to comply with these requirements. New alternatives to both linear [1]–[4] and nonlinear [5]–[8] methods have been proposed using predictive algorithms to achieve high-bandwidth control loops [9].

Linear predictive control algorithms are based on machine equations to obtain a stator voltage vector to be applied on motor terminals. The stator voltage vector is computed to reach a reference signal in one sampling period in a deadbeat way. In [1], the authors use a set of linear equations to calculate the voltage vector to be applied during the following sampling period $\vec{v}_{\mathbf{s}}[\mathrm{k}+1]$. The authors also explain the problem of noncausality which is common to all linear predictive strategies, since future current vector is needed to obtain the voltage vector. Experimental results prove that an incorrect strategy to deal with noncausality results in large overshoot and oscillations on stator current.

Manuscript received May 22, 2008; revised January 22, 2009. First published February 18, 2009; current version published June 3, 2009. This work was supported in part by the Chilean National Fund of Scientific and Technological Development (FONDECYT) under Grant 1060436 and in part by the Universidad Técnica Federico Santa María.

H. Miranda is with the Department of Energy Technology, Aalborg University, 9220 Aalborg East, Denmark (e-mail: hernan.miranda@usm.cl).

P. Cortés, J. I. Yuz, and J. Rodríguez are with the Electronics Engineering Department, Universidad Técnica Federico Santa María, Valparaíso 110-V, Chile (e-mail: patricio.cortes@usm.cl).

Digital Object Identifier 10.1109/TIE.2009.2014904

In [2], Abu-Rub *et al.* design a predictive state-space controller in which the state vector is formed by previous and current stator current errors. The feedback matrix is designed in a deadbeat way, thus obtaining zero stator current error at the next sampling instant. Future variables, in this case the back EMF of an electric machine, are predicted based on current values and past angle increments of this variable.

Robustness of linear predictive controllers is studied in [3], where several deadbeat controllers are designed based on assumptions over future stator current and voltage vectors. In that work, it is shown that deadbeat controllers are not as robust as desired. Two fast $(z = 0)$ and one slower $(z = 0.5)$ poles, i.e., a lower closed loop bandwidth, are used to increase robustness, thus incorporating dynamics and time delays that are not present in the plant model, sacrificing dynamic performance for robustness.

A torque predictive scheme is presented in [4], where the stator flux vector is predicted based on torque demand given by a linear speed controller. With this flux vector, the stator voltage vector is obtained in a deadbeat fashion. Coordinate rotation is also predictively performed using past rotor flux angle changes.

Other applications of deadbeat control have been proposed for current control in single-phase inverters [10], three-phase inverters [11], rectifiers [12], [13], multilevel active rectifiers [14], active filters [15], and uninterruptible power supplies [16]. Recent publications present improvements of the deadbeat controller by including a self-tuning load model [17] and an observer for load uncertainties [18] in order to improve robustness.

Nonlinear predictive strategies have been presented in [5]–[8]. These references are based on Model Predictive Control (MPC) and consider the use of the reduced number of voltage vectors available in a two-level inverter to obtain an optimal actuation signal that minimizes a given function. In [5], the main goal is to obtain control of the stator flux vector. The selected stator voltage vector is applied on motor terminals during the next sampling interval in conjunction with the zero voltage vector in order to minimize the tracking error. The latter is compared to hysteresis and pulsewidth-modulated current control in [6], and used to control the current flowing through a resistive-inductive load driven by a three-level neutral clamped point inverter in [7]. On the other hand, in [8], the authors propose the use of a frequency-dependent cost function in order to obtain an improved current spectrum. Other applications of this kind of controller include active front-end rectifiers [19], [20], multilevel inverters [21], and matrix converters [22], [23].

This paper proposes an MPC with a discrete-time state-space machine model that includes the time-varying rotor speed term, improving the state estimation accuracy, compared to simple Euler approximation. The machine model is updated at every sampling instant and used to predict the future current and flux values for each voltage vector available in a two-level inverter. The voltage vector producing the least torque and stator flux magnitude errors is selected to be applied during the next sampling interval, thus including the inherent nonlinear characteristics of the power drive into the control algorithm. Predictive control has the advantage of presenting a fast dynamic response while the flexible structure of the controller easily allows the inclusion of nonlinearities and constraints in the control law. The use of a cost function gives the control algorithm a high level of flexibility, making possible to include system nonlinearities and constraints in the optimization procedure. As a way of illustration, we show how overcurrent protection can be readily implemented in the control algorithm. In the same way, it is also possible to include additional constraints in the cost function such as reduction of the switching frequency [7] and imposed spectrum [8]. The effect of sampling and delays introduced by the computation time is also discussed. Experimental results for a 4-kW induction machine driven by a two-level inverter are presented proving the feasibility of the proposed motor model.

II. Machine Equations

The control signal for a voltage source inverter is the stator voltage vector $\vec{v}_{\mathbf{s}}$, which is applied to the machine through the stator terminals. Stator variables, voltage $\vec{v}_{\mathbf{s}}$, current $\vec{i}_{\mathbf{s}}$, and flux $\vec{\psi}_{\mathbf{s}}$ are electrically related according to

$$\vec{v}_{\mathbf{s}} = R_{\mathrm{s}}\vec{i}_{\mathbf{s}} + \frac{\vec{\psi}_{\mathbf{s}}}{dt} \tag{1}$$

where R_{s} is the stator resistance. This equation is known as the stator equation.

Rotor equation in a stator fixed reference frame (2) represents the relation between rotor current $\vec{i}_{\mathbf{r}}$ and rotor flux $\vec{\psi}_{\mathbf{r}}$

$$0 = R_{\mathrm{r}}\vec{i}_{\mathbf{r}} + \frac{\vec{\psi}_{\mathrm{r}}}{dt} - j\omega_{\mathrm{m}}\vec{\psi}_{\mathrm{r}} \tag{2}$$

where R_{r} is the rotor resistance and ω_{m} is the rotor speed.

Flux linkage equations (3) and (4) in any coordinate system relate stator and rotor fluxes with stator and rotor currents, where L_{m}, L_{s}, and L_{r} are the mutual, stator, and rotor inductances, respectively,

$$\vec{\psi}_{\mathbf{s}} = L_{\mathrm{s}}\vec{i}_{\mathbf{s}} + L_{\mathrm{m}}\vec{i}_{\mathbf{r}} \tag{3}$$

$$\vec{\psi}_{\mathrm{r}} = L_{\mathrm{m}}\vec{i}_{\mathbf{s}} + L_{\mathrm{r}}\vec{i}_{\mathbf{r}}. \tag{4}$$

Electric torque produced by the induction machine can be expressed in terms of stator current and stator flux

$$T_{\mathrm{e}} = \frac{3}{2}p\vec{\psi}_{\mathbf{s}} \times \vec{i}_{\mathbf{s}} \tag{5}$$

where p is the number of pole pairs.

III. State-Space Machine Modeling

Based on the equations presented above, it is possible to represent the motor behavior using only two internal variables (currents and fluxes) and the stator voltage vector [24]. The reduced set of equations (6), (7), where $k_{\mathrm{r}} = L_{\mathrm{m}}/L_{\mathrm{r}}$, $R_\sigma = R_{\mathrm{s}} + k_{\mathrm{r}}^2 R_{\mathrm{r}}$, $\sigma = 1 - L_{\mathrm{m}}^2/(L_{\mathrm{s}}L_{\mathrm{r}})$, $\tau_\sigma = \sigma L_{\mathrm{s}}/R_\sigma$, and $\tau_{\mathrm{r}} = L_{\mathrm{r}}/R_{\mathrm{r}}$, is used for machine modeling. The selected internal variables are stator current $\vec{i}_{\mathbf{s}}$ and rotor flux $\vec{\psi}_{\mathbf{r}}$ vectors

$$\tau_\sigma \frac{d\vec{i}_{\mathbf{s}}}{dt} + \vec{i}_{\mathbf{s}} = \frac{1}{R_\sigma}\vec{v}_{\mathbf{s}} + \frac{k_{\mathrm{r}}}{R_\sigma}\left(\frac{1}{\tau_{\mathrm{r}}} - j\omega_{\mathrm{m}}\right)\vec{\psi}_{\mathrm{r}} \tag{6}$$

$$\tau_{\mathrm{r}} \frac{d\vec{\psi}_{\mathrm{r}}}{dt} + \vec{\psi}_{\mathrm{r}} = L_{\mathrm{m}}\vec{i}_{\mathbf{s}} + j\omega_{\mathrm{m}}\tau_{\mathrm{r}}\vec{\psi}_{\mathrm{r}}. \tag{7}$$

In order to compute the electric torque developed by the machine, it is necessary to express the stator flux vector $\vec{\psi}_{\mathbf{s}}$ in terms of the internal variables as in

$$\vec{\psi}_{\mathbf{s}} = \sigma L_{\mathrm{s}}\vec{i}_{\mathbf{s}} + \frac{L_{\mathrm{m}}}{L_{\mathrm{r}}}\vec{\psi}_{\mathrm{r}}. \tag{8}$$

It is possible to rewrite (6) and (7) in terms of their real and imaginary components, obtaining a set of four linearly independent equations, which can be represented in state-space form

$$\begin{aligned} \dot{\boldsymbol{x}} &= A\boldsymbol{x} + B\boldsymbol{u} \\ \boldsymbol{y} &= C\boldsymbol{x} \end{aligned} \tag{9}$$

where A, B, and C are matrices of appropriate dimensions and $\boldsymbol{x} = [i_{sd}\ i_{sq}\ \psi_{\mathrm{r}d}\ \psi_{\mathrm{r}q}]^{\mathrm{T}}$, $\boldsymbol{u} = [v_{sd}\ v_{sq}]^{\mathrm{T}}$, $\boldsymbol{y} = [i_{sd}\ i_{sq}\ \psi_{sd}\ \psi_{sq}]^{\mathrm{T}}$.

In order to implement the system (9) in a digital processor, it is necessary to obtain a discrete-time state-space representation of the system. It is worth noting that the matrix A depends on the instantaneous value of the mechanical speed ω_{m} making $A = A(\omega_{\mathrm{m}}(\mathrm{t}))$ a linear time-varying system. Time dependence means that it is not possible to obtain an offline numerical calculation of the discrete-time equivalent system due to the variations on ω_{m}. The solution is to obtain a discrete time-varying model that can be updated at every sampling interval with the new measured value of ω_{m}. The more common methods to obtain a sampled-data representation for the system are direct calculation and Euler approximation (first-order series expansion) [25]. Euler approximation is a simple way to obtain a discrete-time system with similar dynamic behavior response. Direct calculation of the state trajectory from (9) is not as simple as the first-order Euler approximation, but provides a more accurate representation in discrete time (see, for example, [26] and the references therein).

The error introduced by an approximate sampled-data model to represent the underlying continuous-time system is a key aspect in order to obtain a smaller prediction error and, hence, better performance. Details of the discretization process are presented in the Appendix; however, we next present the main ideas used to obtain a sampled-data model. The discrete-time

equivalent of the system (9), when the input is generated by a zero-order hold and all matrices are constant, is given by

$$\begin{aligned} \boldsymbol{x}[\mathrm{k}+1] &= \Phi \boldsymbol{x}[\mathrm{k}] + \Gamma \boldsymbol{u}[\mathrm{k}] \\ \boldsymbol{y}[\mathrm{k}] &= C\boldsymbol{x}[\mathrm{k}] \end{aligned} \tag{10}$$

where

$$\Phi = e^{AT_\mathrm{s}} \tag{11}$$

$$\Gamma = \int_0^{T_\mathrm{s}} e^{A\tau} B d\tau \tag{12}$$

and where T_s is the sampling period.

Given the time-varying nature of the model (as explained above), the instantaneous values of the matrices Φ and Γ must be updated at every sampling interval. In order to obtain these time-varying matrices, we separate the matrix A into two matrices, A_c that does not depend on ω_m, and A_ω whose elements depend on the rotor speed, in this way $A = A_c + A_\omega$. With this, (11) can be expressed as

$$e^{AT_\mathrm{s}} = e^{A_c T_\mathrm{s}} \cdot e^{A_w T_\mathrm{s}}. \tag{13}$$

The matrix $\exp(A_c T_\mathrm{s})$ can be calculated offline since its elements do not change with rotor speed, thus being a time invariant matrix. On the other hand, it is possible to obtain (14), a nearly exact representation of $\exp(A_\omega T_\mathrm{s})$ using the Cayley–Hamilton theorem [25] (more details are provided in the Appendix). Note that this procedure gives an exact discrete-time model if the rotor speed ω_m is constant within the sampling interval. Therefore, mechanical speed variations, although being small, will affect the sampled-data model accuracy. However, we will consider this time-varying discrete-time equivalent model as an exact representation of the system.

The matrix representation of the sampled system (9) depends on the rotor speed ω_m through the terms $\cos(\omega_\mathrm{m} T_\mathrm{s})$ and $\sin(\omega_\mathrm{m} T_\mathrm{s})$. Matrix Φ is constructed by multiplication of the time-invariant part calculated offline and the matrix

$$e^{A_\omega T_\mathrm{s}} = \begin{bmatrix} 1 & 0 & \frac{k_\mathrm{r}}{\sigma L s}\left(1-\cos(\omega_\mathrm{m} T_\mathrm{s})\right) & \frac{kr}{\sigma L_\mathrm{s}}\sin(\omega_\mathrm{m} T_S) \\ 0 & 1 & -\frac{k_\mathrm{r}}{\sigma L_\mathrm{s}}\sin(\omega_\mathrm{m} T_\mathrm{s}) & \frac{k_\mathrm{r}}{\sigma L_\mathrm{s}}\sin(\omega_\mathrm{m} T_\mathrm{s}) \\ 0 & 0 & \cos(\omega_\mathrm{m} T_\mathrm{s}) & -\sin(\omega_\mathrm{m} T_\mathrm{s}) \\ 0 & 0 & \sin(\omega_\mathrm{m} T_\mathrm{s}) & \cos(\omega_\mathrm{m} T_\mathrm{s}) \end{bmatrix}. \tag{14}$$

Using (12), it is possible to calculate the matrix Γ relating the control variable $\boldsymbol{u}$, in this case, the stator voltage $\vec{\boldsymbol{v}}_\mathbf{s}$, with the state vector $\boldsymbol{x}$

$$\Gamma = \frac{T_\mathrm{s}}{\sigma L_\mathrm{s}} \begin{bmatrix} A_c(1,1) & 0 \\ 0 & A_c(2,2) \\ A_c(3,1) & 0 \\ 0 & A_c(4,2) \end{bmatrix} \tag{15}$$

with $A_c(i,j)$ being the term of the matrix A_c in row i and column j.

Finally, considering (8), matrix C is given by

$$C = \begin{bmatrix} 1 & 0 & 0 & 0 \\ 0 & 1 & 0 & 0 \\ \sigma L_\mathrm{s} & 0 & L_\mathrm{m}/L_\mathrm{r} & 0 \\ 0 & \sigma L_\mathrm{s} & 0 & L_\mathrm{m}/L_\mathrm{r} \end{bmatrix}. \tag{16}$$

The set of matrices Φ, Γ, and C will be used to predict the internal behavior of the stator current and flux.

IV. Predictive Control

The machine model obtained in the previous section allows us to estimate the rotor flux vector $\vec{\boldsymbol{\psi}}_\mathbf{r}[\mathrm{k}]$ from the stator current measurements. This model is also used to obtain a prediction of the stator current and rotor flux at the next sampling instant, $\vec{\boldsymbol{i}}^{\boldsymbol{p}}_\mathbf{s}[\mathrm{k}+1]$ and $\vec{\boldsymbol{\psi}}^{\boldsymbol{p}}_\mathbf{r}[\mathrm{k}+1]$ (superscript $\boldsymbol{p}$ for predicted variables), based on a given stator voltage $\vec{\boldsymbol{v}}_\mathbf{s}[\mathrm{k}]$, measured current $\vec{\boldsymbol{i}}_\mathbf{s}[\mathrm{k}]$ and estimated rotor flux $\vec{\boldsymbol{\psi}}_\mathbf{r}[\mathrm{k}]$ at current sampling instant. Using (5) and (8), it is also possible to predict the electric torque developed by the machine $T_\mathrm{e}[\mathrm{k}+1]$ and stator flux $\vec{\boldsymbol{\psi}}^{\boldsymbol{p}}_\mathbf{s}[\mathrm{k}+1]$ for this voltage vector $\vec{\boldsymbol{v}}_\mathbf{s}[\mathrm{k}]$.

The stator voltage vector $\vec{\boldsymbol{v}}_\mathbf{s}$ is applied to the motor terminals by a two-level voltage source inverter. This power drive provides a total of seven different voltage vectors $\vec{\boldsymbol{v}}_\mathbf{0} \ldots \vec{\boldsymbol{v}}_\mathbf{6}$ that can be applied on motor terminals. This reduced set of actuation alternatives allows one to predict the effect that each voltage vector would have on electric torque and stator flux, if it was applied for the next sampling period.

With the predicted values of torque and stator flux, electric torque and stator flux magnitude control is obtained by the minimization of a cost function F for which the inputs are the torque reference T^*_e, the predicted torque $T^\mathrm{p}_{ei}[\mathrm{k}+1]$, reference stator flux $|\vec{\boldsymbol{\psi}}_\mathbf{s}|^*$ and the predicted stator flux $|\vec{\boldsymbol{\psi}}^{\boldsymbol{p}}_{\mathbf{s}\boldsymbol{i}}[\mathrm{k}+1]|$ magnitudes, and the subindex i, meaning it is produced by the stator voltage $\vec{\boldsymbol{v}}_{\boldsymbol{i}}$ with $i = 0 \ldots 6$

$$F = \frac{\left(T^*_\mathrm{e} - T^\mathrm{p}_{ei}[\mathrm{k}+1]\right)^2}{T_n^2} + \frac{\left(|\vec{\boldsymbol{\psi}}_\mathbf{s}|^* - \left|\vec{\boldsymbol{\psi}}^{\boldsymbol{p}}_{\mathbf{s}\boldsymbol{i}}[\mathrm{k}+1]\right|\right)^2}{|\vec{\boldsymbol{\psi}}_{\mathbf{s}\boldsymbol{n}}|^2}. \tag{17}$$

For each stator voltage vector available, this cost function F is evaluated, and the stator voltage $\vec{\boldsymbol{v}}_\mathbf{s}[\mathrm{k}]$ producing the minimum cost is selected to be applied on motor terminals. Weight gains T_n and $|\vec{\boldsymbol{\psi}}_{\mathbf{s}\boldsymbol{n}}|$ correspond to the rated torque value and flux reference during normal speed operation; in this way, torque and flux error have the same weight on the cost function F.

A block diagram of the proposed control scheme is shown in Fig. 1. Here, it can be seen that the torque reference is generated by an external speed control loop while the reference for the stator flux magnitude is kept constant. The basic operation of the predictive controller is summarized by the following steps.

1) Stator currents and rotor speed are measured.
2) These measurements are used for prediction of torque and stator flux for all seven different voltage vectors (Predictive model block).

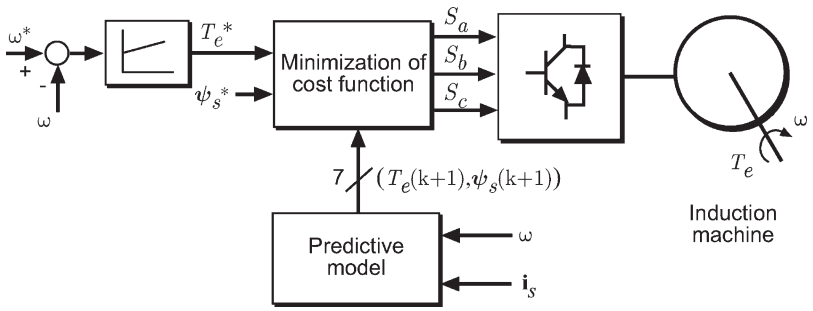

Fig. 1. Predictive torque control diagram.

3) The seven predictions are evaluated using the cost function (Cost function block).
4) The voltage vector that minimizes the cost function is selected and applied in the machine terminals.

These steps are repeated each sampling time, taking into account new measurements and references.

Closed loop control is obtained through the feedback of measurements used for prediction and the action decision taken to minimize the value of the cost function F.

A. Time-Delay Compensation

The predicted values for torque and stator flux magnitude are calculated using the instantaneous value of stator current $\vec{i}_{\mathbf{s}}[\mathrm{k}]$, but the selected stator voltage supposed to generate these predicted values is applied on motor terminals after a whole sampling period, meaning that the stator currents have turned into $\vec{i}_{\mathbf{s}}[\mathrm{k}+1]$, thus diminishing the prediction accuracy.

It is possible to take into account the time delay due to calculations by a two-step prediction. In this way, stator current and rotor flux at sample time $k+1$ (state-space vector $\boldsymbol{x}[\mathrm{k}+1]$) are predicted using the previously calculated stator voltage, i.e., the voltage vector applied at sampling instant k, and measured stator currents, keeping time consistency with sampled currents and voltage applied at the beginning of the sampling interval. The state-space vector at time $k+1$ is used to predict torque and stator flux magnitude at time $k+2$, thus generating the optimal stator voltage vector $\vec{v}_{\mathbf{s}}[\mathrm{k}+1]$. This optimal voltage vector is applied on motor terminals at the beginning of the next sampling period, i.e., when stator current is $\vec{i}_{\mathbf{s}}[\mathrm{k}+1]$, thus overriding the time delay and improving the prediction performance [8]. A flow graph of the control algorithm is shown in Fig. 2. The inputs for the algorithm are the measured current at instant k, the estimated value $\vec{\psi}_{\mathbf{r}}[\mathrm{k}]$, and the selected voltage vector $\vec{v}^{*}_{\mathbf{s}}[\mathrm{k}]$ both calculated in the previous sampling interval.

This way, the cost function must evaluate predictions for time $k+2$ and is redefined as

$$F = \frac{\left(T_{\mathrm{e}}^{*} - T_{\mathrm{e}i}^{\mathrm{p}}[\mathrm{k}+2]\right)^2}{T_n^2} + \frac{\left(|\vec{\psi}_{\mathbf{s}}|^{*} - \left|\vec{\psi}_{\mathbf{s}i}^{\boldsymbol{p}}[\mathrm{k}+2]\right|\right)^2}{|\vec{\psi}_{\mathbf{s}n}|^2}. \quad (18)$$

A simplified diagram with the time instants considered in the control algorithm is shown in Fig. 3. The ideal case is shown in Fig. 3(a) where torque is predicted for a given voltage applied at time k, with currents also measured at time k. However, in the real implementation, the calculation of the optimal voltage needs almost all the sampling period, as shown in Fig. 3(b), and the selected voltage calculated assuming to be applied at time k is applied at time $k+1$. In order to take into account this delay, predictions must consider the actuation to be applied at time $k+1$, and the effect of this voltage in the predicted torque must be evaluated at time $k+2$, as shown in Fig. 3(c).

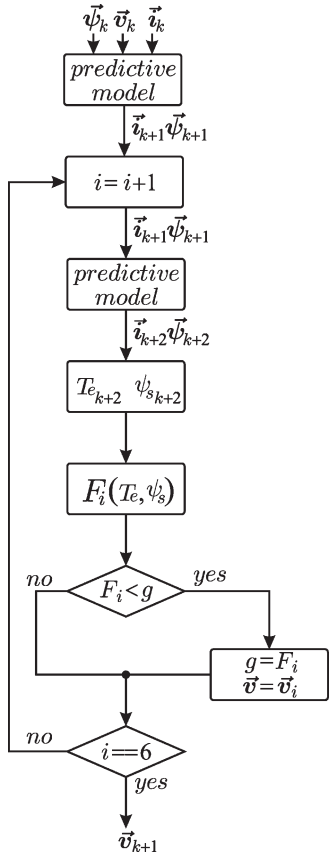

Fig. 2. Control algorithm.

B. Overcurrent Protection

Fast torque or stator flux reference signal changes can produce extremely high stator currents resulting in the destruction of either the motor or the power drive. To ensure that the stator current remains within acceptable bounds, it is possible to make use of the flexibility of the prediction method modifying the cost function (18). A third term that considers the stator current

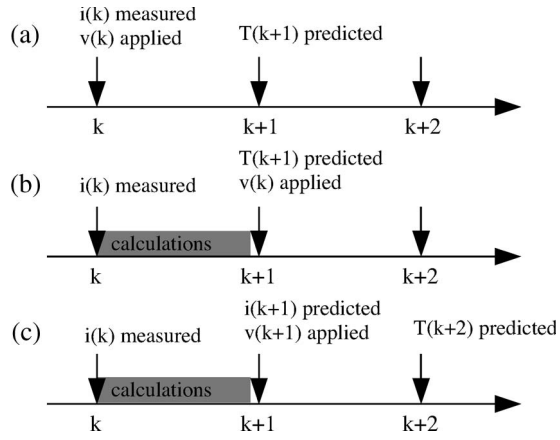

Fig. 3. Time instants for the control algorithm. (a) Ideal case. (b) Real case without compensation. (c) Real case with compensation of the delay.

vector magnitude limit $i_{\max}$ is added with a high weight gain $K_{\rm oc}$ (much larger than $1/T_n^2$ and $1/|\vec{\psi}_{\boldsymbol{sn}}|^2$). The cost function including the overcurrent protection is given by

$$F = \frac{\left(T_{\rm e}^* - T_{ei}^{\rm p}[{\rm k}+2]\right)^2}{T_n^2} + \frac{\left(|\vec{\psi}_{\rm s}|^* - \left|\vec{\psi}_{\boldsymbol{si}}^{\boldsymbol{p}}[{\rm k}+2]\right|\right)^2}{|\vec{\psi}_{\boldsymbol{sn}}|^2} + K_{\rm oc}\left(\left|\vec{i}_{\rm s}^{\boldsymbol{p}}[{\rm k}+2]\right| > i_{\max}\right). \quad (19)$$

Then, if a given stator voltage vector produces an overcurrent, the third term will be equal to $K_{\rm oc}$ and will generate a high value of function F. In this way, this stator voltage vector will not be selected to be applied during the next sampling interval. If the voltage vector under evaluation does not generate an overcurrent state, the third term will be equal to zero, and the cost function is equal to (18).

V. Simulation Results

In order to test the *exact* machine model and compare it to an Euler approximation, a Matlab-Simulink simulation was performed. A zero to rated speed and a speed reversal maneuver were developed. The same vectors applied to the continuous-time machine model were given to the Euler and the exact predictive models. The simulation results are shown in Fig. 4. From top to bottom, the predicted state-space vector is plotted. Stator current prediction is almost the same for both models, while rotor flux direct and quadrature components differ, mainly due to the different structures of the Γ matrix for each discretization method. Comparison was made using the distance to the continuous-time space vector shown in Fig. 5, with error as percentage of the maximum continuous-time vector norm. The error of each model, Euler and *exact*, was tested for the maneuver shown in Fig. 4. As expected, the so-called *exact* discrete-time model has a near zero, less than 0.01% error, produced by the intersample rotor speed variation, while the error for the Euler-based predictive model is over 8% of the maximum state-space vector value.

The effect of the inclusion of overcurrent protection is shown in Fig. 6. It can be seen that when the stator currents are not limited, they can reach very high values during transients, like

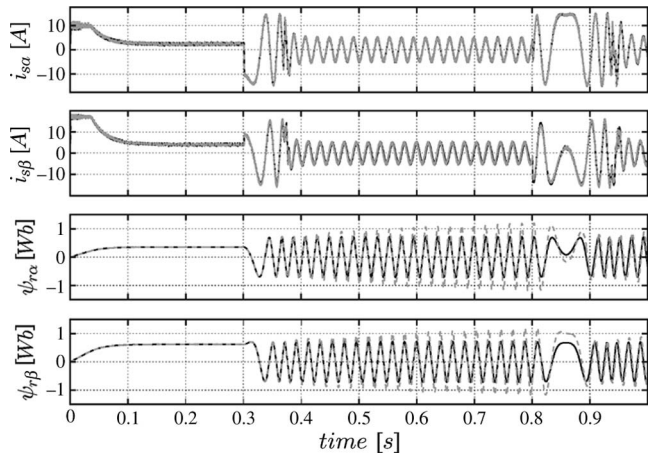

Fig. 4. Simulation result. Predicted state-space vector using (black) exact and (gray and dashed) Euler machine models.

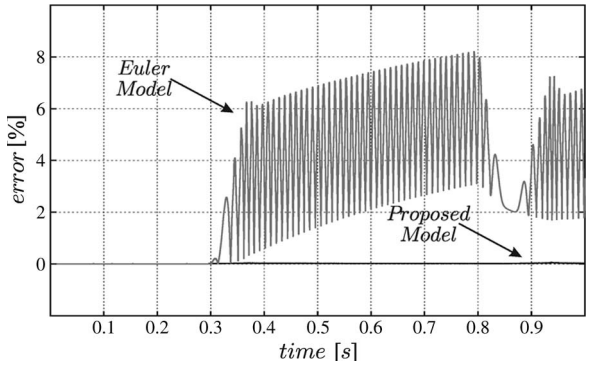

Fig. 5. Simulation result. Prediction error using (gray) Euler and (black) exact machine models.

the machine startup shown here. In order to reach quickly the reference flux magnitude, the currents reach near 30 A. If a limitation of $i_{\max} = 15$ A is considered, using cost function (19), stator currents are clearly limited, as shown in Fig. 6(b).

VI. Experimental Results

The proposed control algorithm was tested experimentally in a two pole-pair 4-kW induction machine. Machine parameters are given in Table I. Sampling frequency for the predictive control algorithm is 20 kHz, while a slow sample of 1-kHz rate has been used for speed control loop to diminish speed measurement noise. Control algorithm and data logging were programmed in a dSPACE 1004 processor; with rotor speed and stator currents measurements as inputs, and firing pulses for a 7-kW two-level inverter as outputs.

Control system response to a step change in speed reference signal is shown in Fig. 7. Speed varies with constant acceleration until the reference value is reached, achieving zero steady-state tracking error. As expected, electric torque signal changes from zero to rated torque with a very fast dynamic response. Once the speed measurement equals the reference value, the torque drops to zero, and the machine operates with constant speed.

Torque response to a step reference change is shown in Fig. 8. Fast dynamic response is achieved with torque rise time (signal

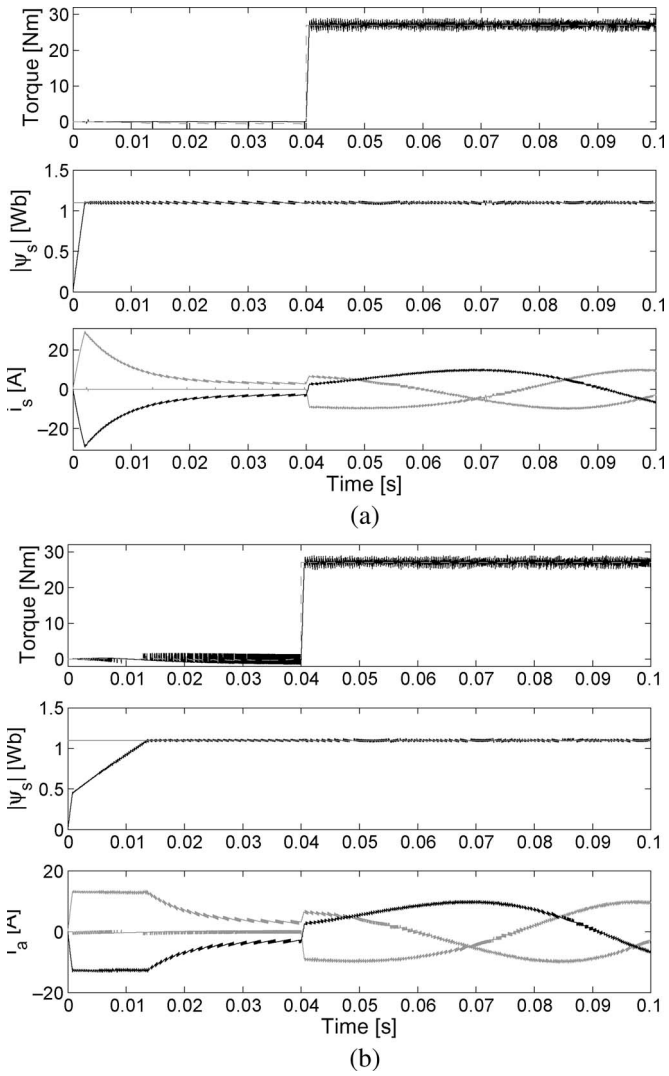

Fig. 6. Simulation results for the overcurrent protection: torque, stator flux magnitude, and stator currents. (a) Without overcurrent protection. (b) With overcurrent protection.

TABLE I
MACHINE PARAMETERS

Parameter	Value	
P_n	4000	[W]
η_n	1440	[RPM]
I_n	9	[A]
V_n	380	[V_{ll}]
R_s	0.97	[Ω]
R_r	1.83	[Ω]
L_s	161	[mH]
L_r	165	[mH]
L_m	154	[mH]
J	0.035*	[Kg/m^2]

* including the load inertia.

reaching 90% of the final value) being less than 0.82 ms. This result clearly confirms the characteristic fast dynamic response of predictive control systems.

A step change from zero to rated torque on mechanical load, with motor operating at 83% rated speed, was applied on rotor shaft using a dc machine driven by a dc chopper. The result of the test is shown in Fig. 9. Once the step change on load torque has been applied, the speed controller raises torque demand in order to keep track of speed reference signal. Load disturbance effect on rotor speed is compensated after 60 ms, and the electric torque developed by the machine equals the load torque value T_l to maintain zero steady-state tracking error.

Modifications of the proposed control, in order to reduce the torque ripple, are under consideration. Some possible solutions include reduction of the sampling time by optimization of the algorithm code, and the use of observers, or a Kalman filter, to reduce the effect of noise in measurements.

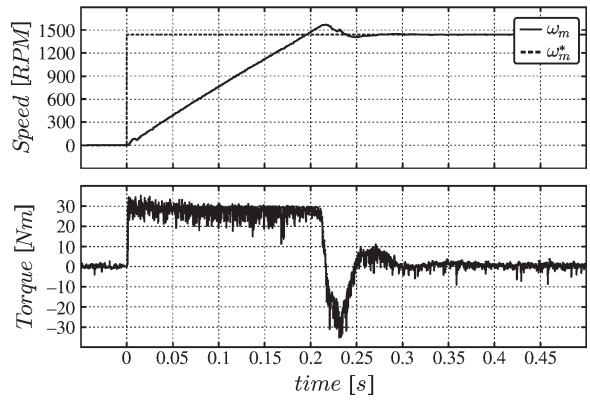

Fig. 7. Experimental result. (Top) Speed and (bottom) estimated torque response to speed reference step change.

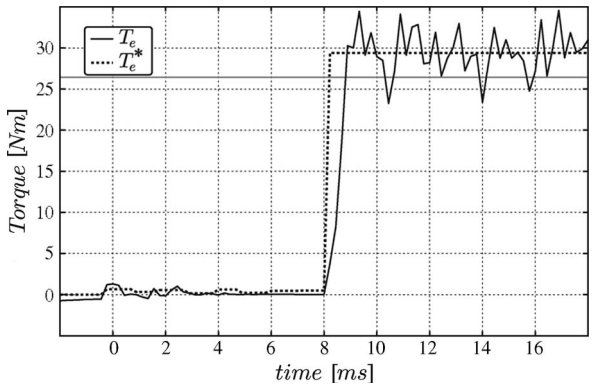

Fig. 8. Experimental result. Estimated torque response to step change on torque reference signal.

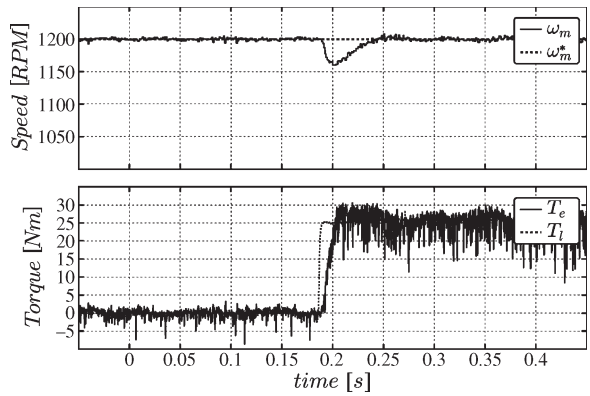

Fig. 9. Experimental result. (Top) Speed and (bottom) estimated torque response to step change on load torque with $\omega_{\rm m} = 0.83\omega_{\rm r}$.

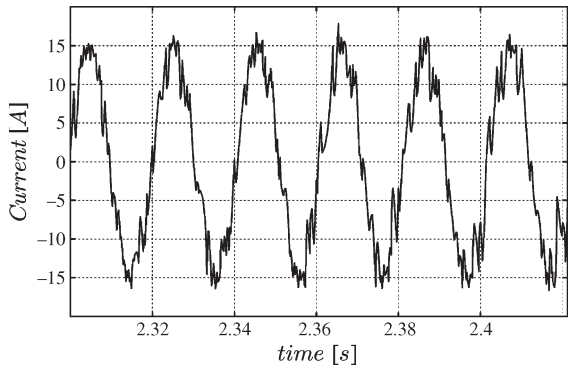

Fig. 10. Experimental result. Stator current with $\omega_{\rm m} = 0.83\omega_n$ and rated load torque.

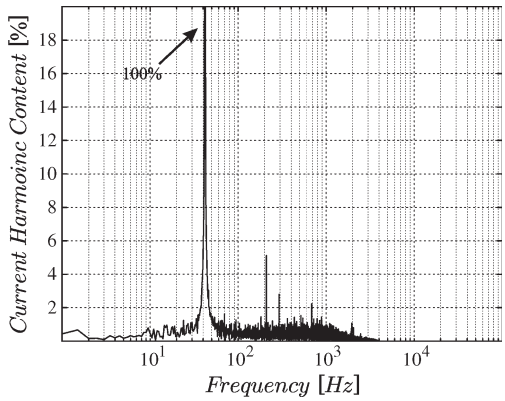

Fig. 11. Experimental result. Stator current spectral content.

Stator current under rated load conditions with rotor operating at $0.83\omega_n$ is shown in Fig. 10. Sinusoidal behavior is clear although no current control loop has been implemented.

Stator current harmonic distortion is shown in Fig. 11 as a percentage of the 42-Hz fundamental component. This measurement was performed using an oscilloscope with sampling frequency of 2 MHz in order to observe high-frequency components. Although no modulation algorithm has been implemented, the harmonic content is kept in relatively low levels, with the most important harmonics being the 5th, 7th, and 17th with magnitudes 5.1%, 2.8%, and 2.2%, respectively. As the switching state of the converter can be changed once at each sampling period, the switching frequency, which is variable, is limited to half the sampling frequency. Then, for a sampling frequency of 20 kHz, it is expected that all harmonic content appear below 10 kHz, as shown in the figure.

VII. Conclusion

A predictive control strategy using a discrete-time state-space model of an induction motor has been developed. The time-varying effect of rotor speed $\omega_{\rm m}$ on the model has been included in order to achieve a more accurate prediction of state variables such as stator flux, rotor flux, and electric torque. Enhanced prediction is achieved and disturbances effect is included in the model by using stator current measurement feedback. The time delay introduced by sampling and computation time has been compensated using a two-step forward prediction algorithm, which improves system performance. The flexibility of the proposed control method is used to include a stator current limit in order to avoid an overcurrent situation.

The experimental results obtained demonstrate the feasibility of the proposed prediction model obtaining a torque control system with fast dynamic response, sinusoidal behavior of stator current, and load torque rejection.

Appendix

Equations (6) and (7) can be rewritten as

$$\frac{d}{dt}\begin{bmatrix}\vec{i}_{\rm s}\\ \vec{\psi}_{\rm r}\end{bmatrix} = \begin{bmatrix} -\frac{1}{\tau_\sigma} & \frac{k_{\rm r}}{\tau_\sigma R_\sigma}\left(\frac{1}{\tau_{\rm r}} - j\omega_{\rm m}\right)\\ \frac{L_{\rm m}}{\tau_{\rm r}} & -\frac{1}{\tau_{\rm r}} + j\omega_{\rm m}\end{bmatrix}\begin{bmatrix}\vec{i}_{\rm s}\\ \vec{\psi}_{\rm r}\end{bmatrix} + \begin{bmatrix}\frac{1}{\tau_\sigma R_\sigma}\\ 0\end{bmatrix}\vec{v}_{\rm s} \tag{20}$$

$$\vec{\psi}_{\rm s} = \begin{bmatrix}\sigma L_{\rm s} & \frac{L_{\rm m}}{L_{\rm r}}\end{bmatrix}\begin{bmatrix}\vec{i}_{\rm s}\\ \vec{\psi}_{\rm r}\end{bmatrix}. \tag{21}$$

Separating real and imaginary components

$$\frac{dx(t)}{dt} = (A_c + A_\omega(t))\,x(t) + Bu(t) \tag{22}$$

$$y(t) = Cx(t) \tag{23}$$

where

$$x(t) = \begin{bmatrix} i_{sd}(t)\\ i_{sq}(t)\\ \psi_{rd}(t)\\ \psi_{rq}(t)\end{bmatrix} \quad u(t) = \begin{bmatrix} v_{sd}(t)\\ v_{sq}(t)\end{bmatrix} \quad y(t) = \begin{bmatrix} i_{sd}(t)\\ i_{sq}(t)\\ \psi_{sd}(t)\\ \psi_{sq}(t)\end{bmatrix} \tag{24}$$

$$A_c = \begin{bmatrix} -\frac{1}{\tau_\sigma} & 0 & \frac{k_{\rm r}}{\tau_\sigma R_\sigma \tau_{\rm r}} & 0\\ 0 & -\frac{1}{\tau_\sigma} & 0 & \frac{k_{\rm r}}{\tau_\sigma R_\sigma \tau_{\rm r}}\\ \frac{L_{\rm m}}{\tau_{\rm r}} & 0 & -\frac{1}{\tau_{\rm r}} & 0\\ 0 & \frac{L_{\rm m}}{\tau_{\rm r}} & 0 & -\frac{1}{\tau_{\rm r}}\end{bmatrix} \tag{25}$$

$$A_\omega(t) = \begin{bmatrix} 0 & 0 & 0 & \frac{k_{\rm r}\omega_{\rm m}(t)}{\tau_\sigma R_\sigma}\\ 0 & 0 & -\frac{k_{\rm r}\omega_{\rm m}(t)}{\tau_\sigma R_\sigma} & 0\\ 0 & 0 & 0 & -\omega_{\rm m}(t)\\ 0 & 0 & \omega_{\rm m}(t) & 0\end{bmatrix} \tag{26}$$

$$B = \begin{bmatrix} \frac{1}{\tau_\sigma R_\sigma} & 0\\ 0 & \frac{1}{\tau_\sigma R_\sigma}\\ 0 & 0\\ 0 & 0\end{bmatrix} \tag{27}$$

$$C = \begin{bmatrix} 1 & 0 & 0 & 0\\ 0 & 1 & 0 & 0\\ \sigma L_{\rm s} & 0 & \frac{L_{\rm m}}{L_{\rm r}} & 0\\ 0 & \sigma L_{\rm s} & 0 & \frac{L_{\rm m}}{L_{\rm r}}\end{bmatrix}. \tag{28}$$

If we assume a piecewise constant input (usually generated by a zero-order hold), and a constant matrix $A(t) = A$, we can obtain from (22) the state transition equation from one sampling instant to the next one [25]

$$x(kT_{\rm s} + T_{\rm s}) = e^{AT_{\rm s}}x(kT_{\rm s}) + \int_0^{T_{\rm s}} e^{A\xi}Bd\xi u(kT_{\rm s}). \tag{29}$$

In our case, matrix $A = A(t) = A_c + A_\omega(t)$ is a time-varying matrix. We obtain an approximate sampled-data model by assuming that the speed $\omega(t)$ and, thus, matrix $A(t)$, are constant between sampling instants. This is

$$x(kT_\mathrm{s} + T_\mathrm{s}) \approx e^{A(kT_\mathrm{s})T_\mathrm{s}} x(kT_\mathrm{s}) + \int_0^{T_\mathrm{s}} e^{A(kT_\mathrm{s})\xi} B d\xi u(kT_\mathrm{s}) \tag{30}$$

where

$$A(kT_\mathrm{s}) = A_c + A_\omega(kT_\mathrm{s}). \tag{31}$$

We then compute the matrix exponential

$$e^{A(kT_\mathrm{s})T_\mathrm{s}} = e^{A_c T_\mathrm{s}} e^{A_\omega(kT_\mathrm{s})T_\mathrm{s}}. \tag{32}$$

The matrix A_c is constant and, thus, the first matrix exponential can be computed offline.

On the other hand, the fact that matrix $A_\omega(t)$ is sparse can be exploited to obtain the second exponential matrix in (32) in terms of $\omega(kT_\mathrm{s})$. Using the Cayley–Hamilton theorem, it can be shown that for the matrix function $\exp(A)$, there exists a polynomial p of degree less than n (n being $\dim(A)$) such that [25]

$$e^A = \alpha_0 I + \alpha_1 A + \cdots + \alpha_{n-1} A^{n-1}. \tag{33}$$

It can be shown [25] that the eigenvalues $\lambda_1 \ldots \lambda_n$ of A are also solutions to (33).

According to this, a polynomial of degree $n = 3$ with coefficients α_0, α_1, α_2, and α_3 dependent of the eigenvalues of A can be computed in order to obtain an exact discrete-time model of the system (9).

The eigenvalues of the matrix $A_\omega T_\mathrm{s}$ are $\lambda_1 = \lambda_2 = 0$, $\lambda_3 = -\lambda_4 = j\omega_\mathrm{m}$. Solving the system of equations given by substitution of λ_1, λ_3, and λ_4 in (33) and λ_2 into the derivative of (33) yields

$$\begin{aligned} \alpha_0 &= 1 \\ \alpha_1 &= 1 \\ \alpha_2 &= \frac{1 - \cos(\omega_\mathrm{m} T_\mathrm{s})}{\omega_\mathrm{m}^2 T_\mathrm{s}^2} \\ \alpha_3 &= \frac{\omega_\mathrm{m} T_\mathrm{s} - \sin(\omega_\mathrm{m} T_\mathrm{s})}{\omega_\mathrm{m}^3 T_\mathrm{s}^3}. \end{aligned} \tag{34}$$

Substitution of $A = A_\omega T_\mathrm{s}$ and the coefficients given in (34) into (33) gives the exact discrete-time form of $\exp(A_\omega T_\mathrm{s})$.

REFERENCES

[1] H. T. Moon, H.-S. Kim, and M.-J. Youn, "A discrete-time predictive current control for PMSM," *IEEE Trans. Power Electron.*, vol. 18, no. 1, pp. 464–472, Jan. 2003.

[2] H. Abu-Rub, J. Guziński, Z. Krzeminski, and H. A. Toliyat, "Predictive current control of voltage-source inverters," *IEEE Trans. Ind. Electron.*, vol. 51, no. 3, pp. 585–593, Jun. 2004.

[3] G. H. Bode, P. C. Loh, M. J. Newman, and D. G. Holmes, "An improved robust predictive current algorithm," *IEEE Trans. Ind. Appl.*, vol. 41, no. 6, pp. 1720–1733, Nov./Dec. 2005.

[4] P. Correa, M. Pacas, and J. Rodríguez, "Predictive control for inverter-fed induction machines," *IEEE Trans. Ind. Electron.*, vol. 54, no. 2, pp. 1073–1079, Apr. 2007.

[5] M. Nemec, D. Nedeljković, and V. Ambrožič, "Predictive torque control of induction machines using immediate flux control," *IEEE Trans. Ind. Electron.*, vol. 54, no. 4, pp. 2009–2017, Aug. 2007.

[6] J. Rodríguez, J. Pontt, C. A. Silva, P. Correa, P. Lezana, P. Cortés, and U. Ammann, "Predictive current control of voltage source inverter," *IEEE Trans. Ind. Electron.*, vol. 54, no. 1, pp. 495–503, Feb. 2007.

[7] R. Vargas, P. Cortés, U. Ammann, J. Rodríguez, and J. Pontt, "Predictive control of a three-phase neutral-point-clamped inverter," *IEEE Trans. Ind. Electron.*, vol. 54, no. 5, pp. 2697–2705, Oct. 2007.

[8] P. Cortés, J. Rodríguez, D. Quevedo, and C. Silva, "Predictive current control strategy with imposed current spectrum," *IEEE Trans. Power Electron.*, vol. 23, no. 2, pp. 612–618, Mar. 2008.

[9] P. Cortes, M. P. Kazmierkowski, R. M. Kennel, D. E. Quevedo, and J. Rodriguez, "Predictive control in power electronics and drives," *IEEE Trans. Ind. Electron.*, vol. 55, no. 12, pp. 4312–4324, Dec. 2008.

[10] H. M. Kojabadi, B. Yu, I. A. Gadoura, L. Chang, and M. Ghribi, "A novel DSP-based current-controlled PWM strategy for single phase grid connected inverters," *IEEE Trans. Power Electron.*, vol. 21, no. 4, pp. 985–993, Jul. 2006.

[11] S.-M. Yang and C.-H. Lee, "A deadbeat current controller for field oriented induction motor drives," *IEEE Trans. Power Electron.*, vol. 17, no. 5, pp. 772–778, Sep. 2002.

[12] L. Malesani, P. Mattavelli, and S. Buso, "Robust dead-beat current control for PWM rectifier and active filters," *IEEE Trans. Ind. Appl.*, vol. 35, no. 3, pp. 613–620, May/Jun. 1999.

[13] Y. Nishida, O. Miyashita, T. Haneyoshi, H. Tomita, and A. Maeda, "A predictive instantaneous-current PWM controlled rectifier with AC-side harmonic current reduction," *IEEE Trans. Ind. Electron.*, vol. 44, no. 3, pp. 337–343, Jun. 1997.

[14] P. Zanchetta, D. B. Gerry, V. G. Monopoli, J. C. Clare, and P. W. Wheeler, "Predictive current control for multilevel active rectifiers with reduced switching frequency," *IEEE Trans. Ind. Electron.*, vol. 55, no. 1, pp. 163–172, Jan. 2008.

[15] J. Mossoba and P. W. Lehn, "A controller architecture for high bandwidth active power filters," *IEEE Trans. Power Electron.*, vol. 18, no. 1, pt. 2, pp. 317–325, Jan. 2003.

[16] P. Mattavelli, "An improved deadbeat control for UPS using disturbance observers," *IEEE Trans. Ind. Electron.*, vol. 52, no. 1, pp. 206–212, Feb. 2005.

[17] Y. A. R. I. Mohamed and E. F. El-Saadany, "An improved deadbeat current control scheme with a novel adaptive self-tuning load model for a three-phase PWM voltage-source inverter," *IEEE Trans. Ind. Electron.*, vol. 54, no. 2, pp. 747–759, Apr. 2007.

[18] Y. A. R. I. Mohamed and E. F. El-Saadany, "Robust high bandwidth discrete-time predictive current control with predictive internal model—A unified approach for voltage-source PWM converters," *IEEE Trans. Power Electron.*, vol. 23, no. 1, pp. 126–136, Jan. 2008.

[19] P. Cortes, J. Rodriguez, P. Antoniewicz, and M. Kazmierkowski, "Direct power control of an AFE using predictive control," *IEEE Trans. Power Electron.*, vol. 23, no. 5, pp. 2516–2523, Sep. 2008.

[20] P. Antoniewicz and M. Kazmierkowski, "Virtual-flux-based predictive direct power control of AC/DC converters with online inductance estimation," *IEEE Trans. Ind. Electron.*, vol. 55, no. 12, pp. 4381–4390, Dec. 2008.

[21] M. Perez, P. Cortes, and J. Rodriguez, "Predictive control algorithm technique for multilevel asymmetric cascaded h-bridge inverters," *IEEE Trans. Ind. Electron.*, vol. 55, no. 12, pp. 4354–4361, Dec. 2008.

[22] R. Vargas, J. Rodriguez, U. Ammann, and P. Wheeler, "Predictive current control of an induction machine fed by a matrix converter with reactive power control," *IEEE Trans. Ind. Electron.*, vol. 55, no. 12, pp. 4362–4371, Dec. 2008.

[23] R. Vargas, U. Ammann, J. Rodriguez, and J. Pontt, "Predictive strategy to control common-mode voltage in loads fed by matrix converters," *IEEE Trans. Ind. Electron.*, vol. 55, no. 12, pp. 4372–4380, Dec. 2008.

[24] J. Holtz, "The representation of AC machine dynamics by complex signals flow graphs," *IEEE Trans. Ind. Electron.*, vol. 42, no. 3, pp. 263–271, Jun. 1995.

[25] K. J. Åstrom and B. Wittenmark, *Computer-Controlled Systems*. Englewood Cliffs, NJ: Prentice-Hall, 1997.

[26] J. I. Yuz and G. C. Goodwin, "On sampled-data models for nonlinear systems," *IEEE Trans. Autom. Control*, vol. 50, no. 10, pp. 1477–1489, Oct. 2005.

Hernán Miranda (S'06) was born in Valparaíso, Chile, in 1979. He received the Electrical Engineering title and Ms.Cs. degree in electronics engineering from the Universidad Técnica Federico Santa María, Valparaíso, in 2004 and 2007, respectively. He is currently working toward the Ph.D. degree in the Department of Energy Technology, Aalborg University, Aalborg, Denmark.

Between 2002 and 2008, he was a Scientific Assistant with the Power Electronics Research Group, Universidad Técnica Federico Santa María. His main research areas include induction machine drives, renewable energy sources, and grid connection of high-power converters.

Patricio Cortés (S'05–M'08) received the B.Eng. and M.Sc. degrees in electronics engineering in 2004 and the Ph.D. degree in 2008 from the Universidad Técnica Federico Santa María (UTFSM), Valparaíso, Chile.

Since 2003, he has been with the Electronics Engineering Department, UTFSM, where he is currently a Research Associate. In 2007, he visited the Institute of Control and Industrial Electronics, Warsaw University of Technology, Warsaw, Poland. His main research interests include power electronics, adjustable-speed drives, and predictive control. He received the Best Paper Award from the IEEE TRANSACTIONS ON INDUSTRIAL ELECTRONICS for 2007.

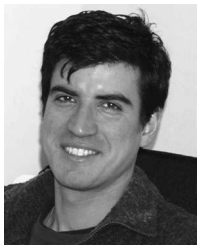

Juan I. Yuz (S'01–M'06) was born in Valparaíso, Chile, in 1975. He received the Ingeniero Civil Electrónico and M.S. degrees in electronics engineering from the Universidad Técnica Federico Santa María (UTFSM), Valparaíso, in 2001, and the Ph.D. degree in electrical engineering from The University of Newcastle, Newcastle, Australia, in 2006.

He currently holds a research position with the Automatic Control Group in the Electronics Engineering Department, UTFSM. His research areas are in control and identification of sampled-data systems.

Dr. Yuz was the recipient of the Best Electronics Engineering Student Award from UTFSM in 2001.

José Rodríguez (M'81–SM'94) received the B.Eng. degree in electrical engineering from the Universidad Técnica Federico Santa María (UTFSM), Valparaíso, Chile, in 1977, and the Dr.-Ing. degree in electrical engineering from the University of Erlangen, Erlangen, Germany, in 1985.

Since 1977, he has been with the Electronics Engineering Department, UTFSM, where from 2001 to 2004, he was the Director and, currently, is a Professor. From 2004 to 2005, he was the Vice-Rector of Academic Affairs, and since 2005, has been the Rector at UTFSM. During his sabbatical leave in 1996, he was responsible for the Mining Division, Siemens Corporation, Santiago, Chile. He has extensive consulting experience in the mining industry, particularly in the application of large drives such as cycloconverter-fed synchronous motors for SAG mills, high-power conveyors, and controlled ac drives for shovels and power-quality issues. He has directed more than 40 R&D projects in the field of industrial electronics. He has coauthored more than 250 journal and conference proceedings papers and contributed one book chapter. His research group has been recognized as one of the two Centers of Excellence in Engineering in Chile from 2005 to 2008. His main research interests include multilevel inverters, new converter topologies, and adjustable-speed drives.

Prof. Rodríguez has been an active Associate Editor of the IEEE TRANSACTIONS ON POWER ELECTRONICS and IEEE TRANSACTIONS ON INDUSTRIAL ELECTRONICS, since 2002. He has served as Guest Editor for the IEEE TRANSACTIONS ON INDUSTRIAL ELECTRONICS in five instances [Special Sections on matrix converters (2002), multilevel inverters (2002), modern rectifiers (2005), high-power drives (2007), and predictive control of power converters and drives (2008)]. He received the Best Paper Award from the IEEE TRANSACTIONS ON INDUSTRIAL ELECTRONICS for 2007.